

We are IntechOpen, the world's leading publisher of Open Access books Built by scientists, for scientists

6,900

Open access books available

186,000

International authors and editors

200M

Downloads

Our authors are among the

154

Countries delivered to

TOP 1%

most cited scientists

12.2%

Contributors from top 500 universities



WEB OF SCIENCE™

Selection of our books indexed in the Book Citation Index
in Web of Science™ Core Collection (BKCI)

Interested in publishing with us?
Contact book.department@intechopen.com

Numbers displayed above are based on latest data collected.
For more information visit www.intechopen.com



Waveform Capnography for Monitoring Ventilation during Cardiopulmonary Resuscitation: The Problem of Chest Compression Artifact

Mikel Leturiondo, Sofía Ruiz de Gauna, José Julio Gutiérrez, Digna M. González-Otero, Jesus M. Ruiz, Luis A. Leturiondo and Purificación Saiz

Abstract

Sudden cardiac arrest (SCA) is the sudden cessation of the heart's effective pumping function, confirmed by the absence of pulse and breathing. Without appropriate treatment, it leads to sudden cardiac death, considered responsible for half of the global cardiac disease deaths. Cardiopulmonary resuscitation (CPR) is a key intervention during SCA. Current resuscitation guidelines emphasize the use of waveform capnography during CPR in order to enhance CPR quality and improve patient outcomes. Capnography represents the concentration of the partial pressure of carbon dioxide (CO₂) in respiratory gases and reflects ventilation and perfusion of the patient. Waveform capnography should be used for confirming the correct placement of the tracheal tube and monitoring ventilation. Other potential uses of capnography in resuscitation involve monitoring CPR quality, early identification of restoration of spontaneous circulation (ROSC), and determination of patient prognosis. An important role of waveform capnography is ventilation rate monitoring to prevent overventilation. However, some studies have reported the appearance of high-frequency oscillations synchronized with chest compressions superimposed on the capnogram. This chapter explores the incidence of chest compression artifact in out-of-hospital capnograms, assesses its negative influence in the automated detection of ventilations, and proposes several methods to enhance ventilation detection and capnography waveform.

Keywords: cardiopulmonary resuscitation, advanced life support, waveform capnography, ventilation, chest compression artifact

1. Introduction

In the past century, cardiac disease was declared as one of the leading causes of global death, comprising a 30% of the global mortality [1]. It is estimated that

sudden cardiac death is responsible for half of all cardiac disease deaths [1, 2], affecting more than 300,000 victims per year in the United States and around 275,000 in the Europe [3–5]. About 80% of sudden cardiac deaths are caused by out-of-hospital cardiac arrests (OHCA) [1], defined as the sudden cessation of the heart's effective pumping function confirmed by the absence of pulse and breathing and occurring in an out-of-hospital setting [6].

During OHCA, there are two prehospital life supporting emergency medical services (EMS): basic life support (BLS) and advanced life support (ALS). BLS treatment is provided by emergency medical technicians and includes early CPR and early defibrillation, usually delivered with an automated external defibrillator (AED). ALS treatment procured by clinicians during CPR usually includes manual defibrillation, advanced airway placement, and drug administration, together with CPR [7, 8].

Several studies have reported a strong correlation between the quality of CPR and the chance of successful defibrillation [9–11]. Thus, resuscitation guidelines [12, 13] globally recommend providing chest compressions with a rate in the range of 100 and 120 compressions per minute (cpm) and achieving a depth between 5 and 6 cm. Ventilations should be provided with a 30 compressions-to-2 ventilations ratio before intubation. After intubation, ALS guidelines recommend continuous chest compressions and ventilations with a ventilation rate around 10 breaths per minute [7, 8]. Despite the fact that some studies have declared hyperventilation as harmful for patient outcome, by either high rate or volume [14, 15], excessive ventilation rates (as high as 30 breaths per minute) are common in resuscitation [16–18]. Many animal studies revealed that high ventilation rates increased intrathoracic pressures and decreased coronary perfusion and survival rates [16, 19, 20]. However, another recent animal study reported no adverse hemodynamic effects, although they did observe a decrease in maximum CO₂ values [21].

In order to alleviate this problem and prevent inadvertent hyperventilation, resuscitation guidelines highlight the role of capnography for ventilation rate monitoring during CPR [7, 8]. Other advantages of capnography include assessment of the correct placement of the endotracheal tube [21], monitoring the quality of chest compressions [22], early identification of restoration of spontaneous circulation (ROSC) [23], and determination of patient prognosis [7, 24, 25].

This chapter analyzes the use of capnometry for ventilation monitoring during OHCA episodes. First, we briefly introduce the evolution of capnometry and the different technologies used in the field. Then, we characterize the capnography signal during ongoing CPR. The main conclusion of this analysis is that the appearance of high-frequency oscillations superimposed on the waveform capnography is frequent during resuscitation. We then analyze the impact of these oscillations on out-of-hospital automated detection of ventilations. Finally, we propose two methods to improve ventilation detection during CPR by filtering the artifact from the capnography signal and a method to enhance capnography waveform in the presence of artifact.

2. Evolution of capnometry

Since 1943, capnometry has become an essential component of standard anesthesia monitoring [26]. Capnometry represents the numerical value of the carbon dioxide (CO₂) partial pressure measurement in exhaled respiratory gases. The maximum CO₂ concentration at the end of the exhalation, known as end-tidal CO₂ (ETCO₂), reflects cardiac output and pulmonary blood flow. Preventing hypoxia, i.e., deprivation of adequate oxygen supply, during anesthesia is the primary goal of

anesthesiologists. Improvements with capnometry in this field currently allow the early identification of harmful situations before hypoxia leads to irreversible brain damage. Because of these improvements, the use of capnography has spread from the operating room into emergency medicine environment and even into out-of-hospital emergency settings.

Several methods have been used to determine the presence and concentration of CO₂ over the years. The simplest form of CO₂ detection available is colorimetric capnometry. This technology is based on a paper that changes in color in the presence of CO₂, but its inability to detect breath-to-breath changes prohibits the use of this device to guide ventilation. Later, semiquantitative capnometers (**Figure 1a**) that provide a rough estimation of the ET_{CO}₂ concentration have been developed. The technology behind these devices reports the ET_{CO}₂ value in a series of stacked colors rather than providing a numerical value, being useful to confirm correct airway placement.

More recently, quantitative capnometry involving infrared spectrophotometric analysis of expired gases (**Figure 1b**) has led to the most accurate method to measure ET_{CO}₂ values. This technology provides an end-tidal value for each breath, allowing an optimal control of ventilation. Improvements in the field allowed the graphical representation and recording of the CO₂ concentration throughout the breath (i.e., waveform capnography, **Figure 1c**).

Two different methods of gas sampling, illustrated in **Figure 2**, are used to measure quantitative capnometry and waveform capnography: mainstream and sidestream. The main difference is that mainstream is directly placed in the main flow of exhaled gases, while in sidestream little samples are aspirated with a capillary sampling tube. During the last two decades, improvements in high-flow sidestream capnometers turned into Microstream™ capnometers, with an aspiration flow rate of 50 ml min⁻¹. This technology uses a highly CO₂-specific infrared source where

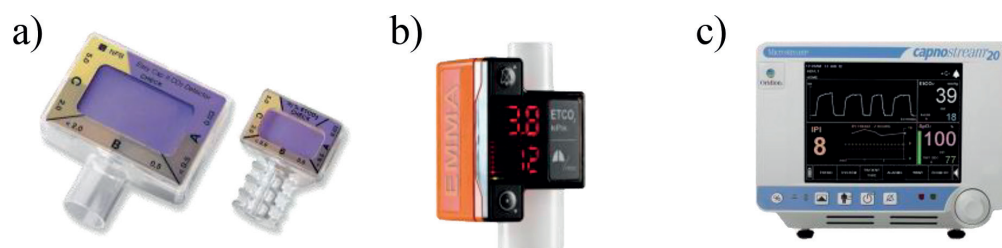


Figure 1. Evolution of capnometry in out-of-hospital emergency settings. (a) Semiquantitative capnometer, (b) quantitative capnometer, and (c) waveform capnography. Courtesy of Medtronic and Masimo.

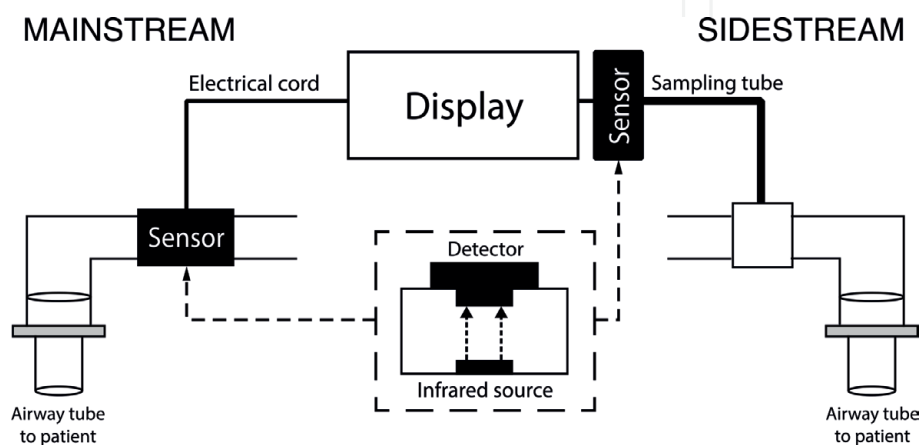


Figure 2. Brief schemes of quantitative capnometry to acquire the capnography signal, mainstream and sidestream.

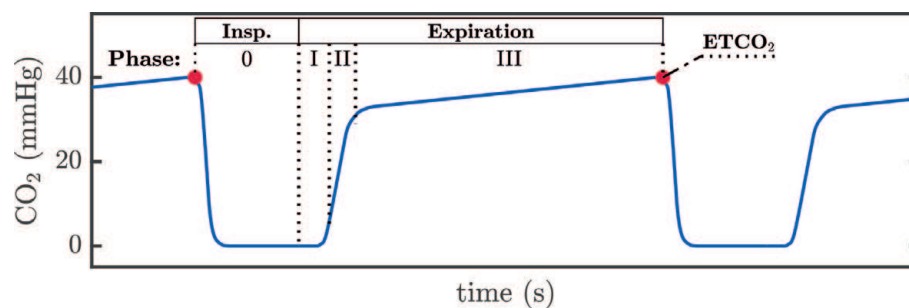


Figure 3.

The normal capnogram. Capnography waveform representing the variation of CO_2 concentration during the respiratory cycle. Segments and phases follow the nomenclature proposed by Bhavani-Shankar and Philip [27].

the IR emitter exactly matches the absorption spectrum of the CO_2 molecules. This facilitates the sample cell to use a much smaller volume that permits a low flow rate, being less likely to aspirate water and secretions.

The evolution and morphology of CO_2 concentration in the respiratory cycle of a normal capnogram are depicted in **Figure 3**. The initial rapid decrease of CO_2 concentration named as phase 0 represents the inspiration segment, where the lungs are filled with CO_2 -free respiratory gases until a zero level is reached, defining the baseline of the capnogram. The following phases represent the expiration segment: during phase I, the CO_2 -free gas in the anatomical dead space (between the alveoli and measurement device) is exhaled; in phase II a mixture of gases from the anatomical dead space and the alveoli quickly rises the level of CO_2 concentration; finally in phase III, CO_2 -rich gases coming from the alveoli slowly raise the CO_2 concentration until a peak level is reached, corresponding to the ETCO_2 value [28].

3. Capnography signal during ongoing chest compressions

The initial use of capnographs during resuscitation was initially proposed by the International Liaison Committee on Resuscitation (ILCOR) in 2010, and since 2015 it is becoming a standard of care in advanced high-quality CPR [24, 29, 30]. Among the several advantages of waveform capnography during CPR emphasized in current resuscitation guidelines, but one of its most important roles is to monitor ventilation rate, helping to avoid overventilation.

For a reliable clinical analysis, either visual or automated, of the waveform capnography, its morphology is essential. All phases of the respiratory cycle must be identifiable during CPR, and the measurement of ETCO_2 should be possible. However, issues related to the capnograph as well as to the ongoing resuscitation efforts may distort the waveform capnography [29, 31, 32]. Moreover, the appearance of fast oscillations induced in the waveform capnography at different rates and with varying amplitude has been reported in several studies [33–35], often completely distorting the real tracing of the respiratory cycle as shown in **Figure 4b**.

To the best of our knowledge, studies assessing the incidence and origin of this artifact are sparse. A preliminary abstract published by Idris et al. [33] in 2010 analyzed a dataset of 210 patients and detected the presence of this artifact in 154 episodes, reporting an incidence greater than 70%. Several studies found that provided chest compressions generate passive ventilations of low inspiratory tidal volumes [33–35]. Deakin et al. [34] found that generated low tidal volumes during ongoing chest compressions were considerably lower than the anatomical dead space (150 ml). Recently, Vanwulpen et al. [35] conducted a similar out-of-hospital study, and their results were in line with the ones reported by Deakin et al., but they found lower inspiratory volumes. Therefore generated gas exchange is insufficient to properly ventilate the patient [36].

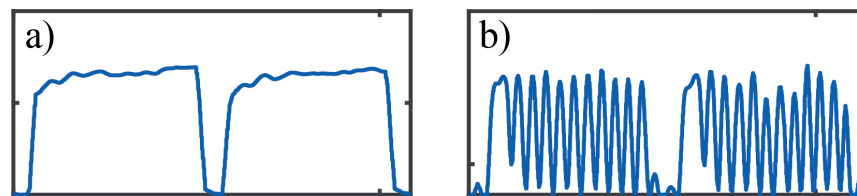


Figure 4. OHCA waveform capnography signal segments. (a) Nondistorted waveform and (b) capnogram distorted by fast oscillations.

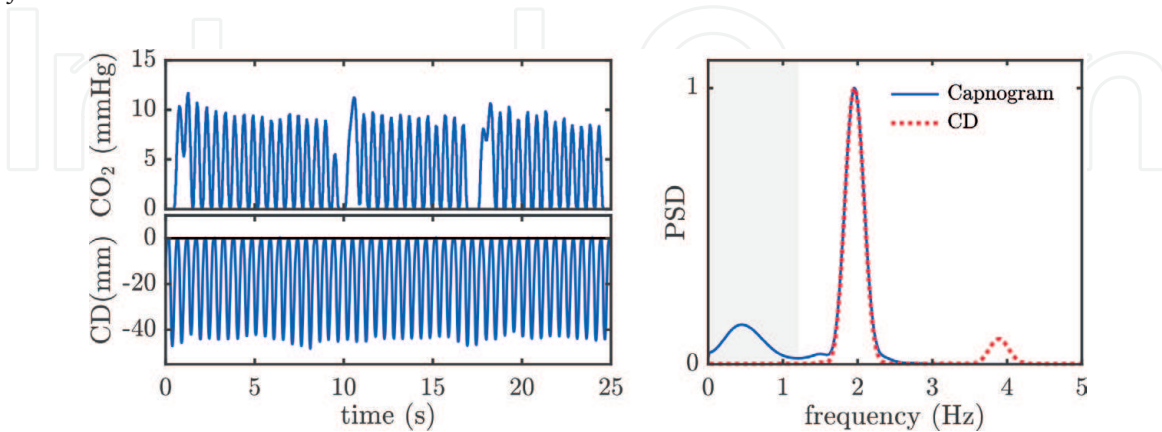


Figure 5. Time-domain and spectral analyses of the oscillations present in a capnogram segment (top left). CD signal (bottom left). Normalized PSD analysis (right) of the distorted capnogram (solid blue) and of the CD signal (dotted red). The high-frequency peak around 2 Hz matches the average chest compression rate of 116 compressions per minute.

Our first approach was to assess the origin of the artifact, so we performed time-domain and spectral analyses on a large set of out-of-hospital capnograms. Readers are encouraged to consult reference [37] for further details. As an example, **Figure 5** depicts a distorted capnogram interval (top-left panel), the concurrent chest compression depth (CD) signal (bottom-left panel), and the normalized power spectral density (PSD) estimated (right panel) for both the waveform capnography signal (solid blue) and for the CD signal (dotted red). The PSD analysis of the waveform capnography reveals a low-frequency peak that represents the ventilation rate (shadowed in gray) and a high-frequency peak corresponding to the artifact oscillation frequency. The latter exactly overlaps with the fundamental frequency peak of the CD signal. Thus, the induced artifact presents a sinusoidal pattern with a fundamental frequency that matches the frequency of the chest compressions.

The appearance of the artifact induced by chest compressions can negatively affect the quality of CPR in three different aspects: first, causing misdetection of ventilations and consequently giving an incorrect feedback in the estimation of ventilation rate; second, impeding reliable and stable ETCO₂ measurements as reported by Raimondi et al. [38]; and third, interfering with CPR providers' waveform capnography interpretation.

4. Impact of chest compression artifact on ventilation detection

This section briefly describes the conducted analysis to characterize the morphology of the chest compression-induced oscillations and assess its impact on automated ventilation detection during ongoing CPR. First, we describe the process followed to collect the OHCA episodes used in the study, as well as the steps followed to annotate each ventilation instance. Then, we describe an algorithm designed to automatically detect ventilations in the capnogram. Finally, we assess

the impact of the artifact on the reliability of ventilation detection by testing the performance of the detection algorithm. For a more detailed description of the database used and the methods followed, see Ref. [37].

4.1 Data collection and annotation

In order to perform the analysis, a dataset of 301 episodes was selected from a large database collected between 2011 and 2016 as part of the Resuscitation Outcomes Consortium (ROC), collected by the Portland Regional Clinical Centre (Oregon, USA). The data collection was approved by the Oregon Health and Science University (OHSU) Institutional Review Board (IRB00001736). No patient private data was required for this study. Episodes were recorded using Heartstart MRx monitor-defibrillators (Philips, USA), equipped with real-time CPR feedback technology (Q-CPR) and sidestream waveform capnography (Microstream, Oridion Systems Ltd., Israel). Ventilation was provided with a bag valve mask (BVM), endotracheal tube (ETT), or the King LT-D supraglottic airway (SGA).

Three biomedical engineers participating in the study visually reviewed and manually annotated each OHCA episode. Episodes were classified as distorted if evident chest compression-induced oscillations were found during more than 1 min of the total chest compression time. In the case of distorted episodes, experts annotated the location of the artifact with respect to the capnogram segment to characterize its morphology. Otherwise, episodes were grouped as nondistorted. Episodes and intervals with unreliable data caused by excessive noise or disconnections were discarded.

Figure 6 shows an example of the ventilation annotation process. The compression depth (CD) signal (top panel) was used to determine whether chest compressions were provided or not. The position of each single ventilation was also annotated using the TI signal as a reference. Provided ventilations provoke slow fluctuations in the TI signal [39–41]. The raw TI signal was low-pass filtered to enhance the slow fluctuations caused by ventilations (middle panel, blue line). Each ventilation was annotated at the instant corresponding to a rise in each impedance

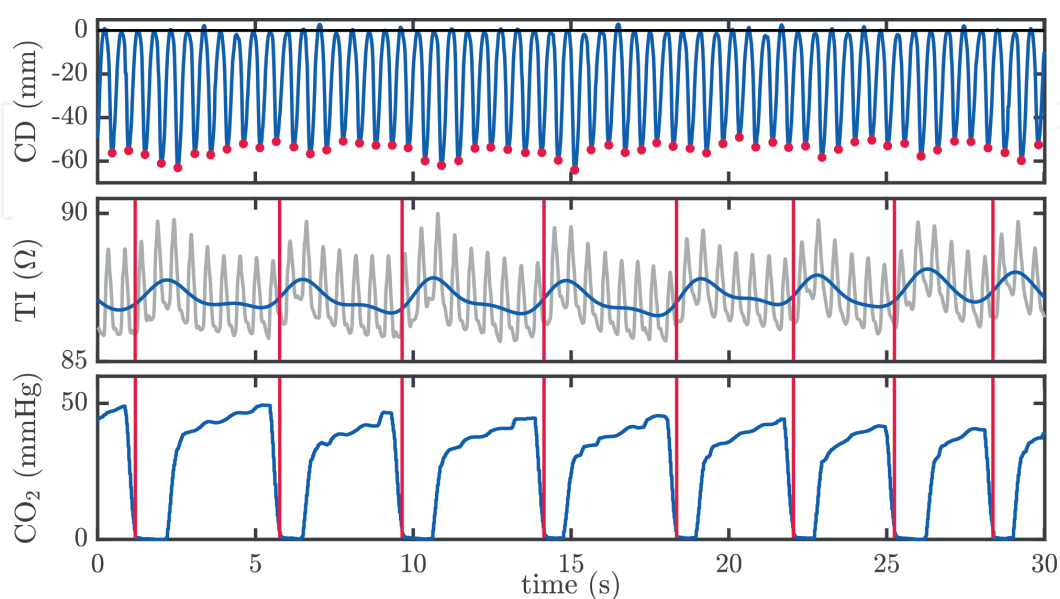


Figure 6. CD signal measured with Q-CPR technology (top panel), raw TI signal acquired through defibrillation pads (middle panel, gray line) and waveform capnography (bottom panel). Using the low-pass filtered TI signal (middle panel, blue line), ventilations were annotated at the rise of a TI fluctuation, corresponding with a CO_2 rapid decay to zero.

fluctuation (vertical red line). The capnogram depicted in the bottom panel allows visual confirmation of the presence of ventilations. Resulting annotations were used as the gold standard to evaluate the performance of an automated capnogram-based ventilation detection algorithm.

4.2 Method for an automated capnogram-based ventilation detection

There is remarkably little knowledge about how the proprietary algorithm of a commercial capnometer works. In 2010, Edelson et al. [41] proposed the first algorithm to automatically detect ventilations in the capnogram during CPR. For this study, we designed a new algorithm for ventilation detection, based upon certain assumptions about the nature of the CO₂ waveform.

A simplified scheme of the algorithm performance is shown in **Figure 7**. The algorithm searches for series of consecutive upstrokes (t_{up}) and downstrokes (t_{dw}) in the capnogram. These abrupt changes are detected when the amplitude of the capnogram exceeds or goes below a fixed threshold, Th_{amp} (mmHg). Then the algorithm extracts two features, the duration between consecutive abrupt changes, considered as an estimation of expiration and inspiration intervals, D_{ex} and D_{in} . Classification of potential true ventilations is done according to a simple decision tree based on Th_{ex} and Th_{in} thresholds. If both duration features are greater than these thresholds, the ventilation is annotated at the instant when the downstroke occurs (t_{dw}).

The performance of the algorithm was evaluated in terms of its sensitivity (Se) and positive predictive value (PPV). Se was defined as the proportion of annotated ventilations that were identified by the algorithm and PPV as the proportion of detected ventilations that were true ventilations. Ventilation detection instances were matched with the gold standard annotations if they were within ± 0.5 s of one another. The algorithm was first trained with a subset of 30 nondistorted episodes obtaining the maximizing Se while assuring a PPV >98%. Ventilation detection performance was reported for the remaining episodes (test set), consisting of a mixture of distorted and nondistorted episodes.

In order to assess how the ventilation rate estimation is influenced by the chest compression artifact, we computed, for each episode in the whole set, the number of ventilations given during every minute, using a 1-minute sliding window with an

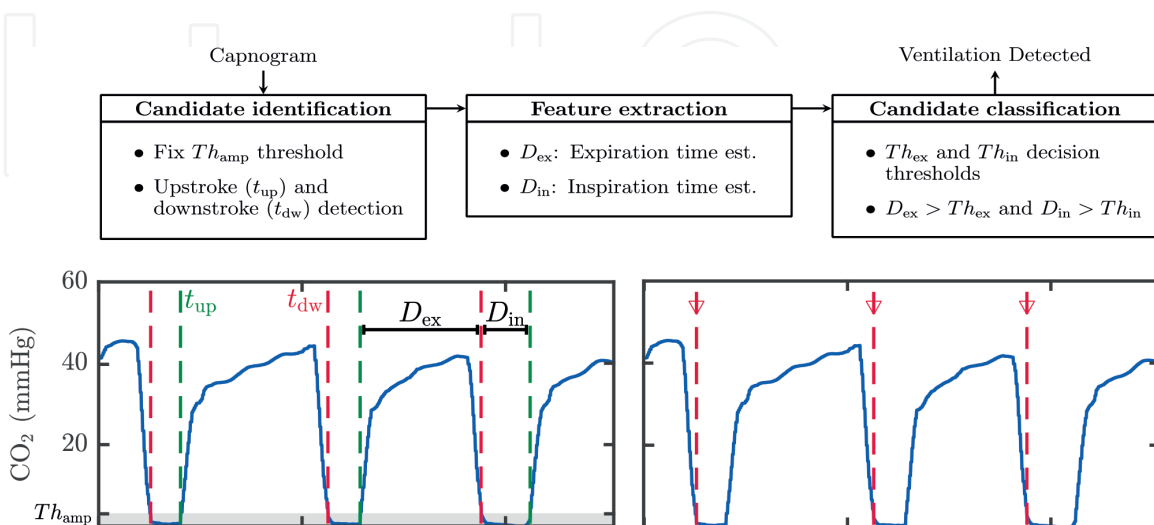


Figure 7. The ventilation detection scheme is described in the top panel. Applying a fixed amplitude threshold Th_{amp} the algorithm searches consecutive upstrokes (t_{up}) and downstrokes (t_{dw}) in the waveform capnography signal (bottom-left panel). Then, it extracts the duration of the intervals D_{ex} and D_{in} . Finally, features greater than the fixed duration thresholds Th_{ex} and Th_{in} are classified as true ventilations. Detected ventilations are depicted with vertical red dotted lines (bottom-right panel).

overlap factor of 1/6. Hence, ventilation rate value was updated every 10 s. Then, we compared the ventilation rate measurements estimated from the ventilation detections with those computed from the gold standard annotations. Using the computed ventilation rate per minute measurements, we also calculated the overventilation alarms obtained for a 10 min^{-1} threshold. Then, we tested the ability of our algorithm to correctly detect overventilation.

Results were reported as mean (\pm SD) if they passed Lilliefors normality test and as median (IQR) otherwise. Distribution of Se and PPV per record and distributions of the percent error in the estimation of ventilation rate were depicted with box plots, which graphically report median, IQR, and possible outlier values.

4.3 Characterization of chest compression artifact and ventilation detection performance

From the original dataset of 301 episodes, 23% were discarded (69 records) due to unreliable waveform capnography or TI signals. Permanent signal disconnection or saturation, capnograms without respiratory cycle variations or under 5 mmHg during the whole episode (32 records), and inability to observe ventilation fluctuations in the filtered TI signal (20 records) were some of the reasons for elimination. Remaining 232 episodes had a mean duration of 30 (\pm 9.5) min per episode.

A total of 98 episodes (42%) were annotated as distorted. The artifact was classified into three types: type I, observed primarily during the expiratory plateau; type II, in the capnogram baseline; and type III, spanning from the plateau to the baseline. No induced chest compression oscillations were found in the slopes of phases 0 and II. **Figure 8** depicts, for each artifact type, examples of capnogram intervals observed during ongoing chest compressions. The ventilation annotation process yielded a total of 52,654 ventilation instances, with a mean of 227 (\pm 118) ventilations per episode. Nondistorted episodes comprised 30,814 ventilations and distorted episodes 21,840 ventilations (type I, 10,119; type II, 5228; and type III, 6493).

Global Se was 96.4% and PPV was 95.0% for the whole test subset. Reported performance for nondistorted episodes was higher, Se was 99.6%, and PPV was 99.0%. However, performance decreased for the distorted subset, with values of Se and PPV of 91.9 and 89.5%, respectively. This phenomenon is highly noticeable in the case of type III episodes, where performance was drastically affected by the artifact, reporting values of Se and PPV of 77.6 and 73.5%, respectively. **Figure 9** (left panels) shows the performance results of the automated ventilation detection. **Figure 9** (right panel) shows the distribution of the unsigned percent error in the estimation of ventilation rate per episode. For the nondistorted episodes, median error was 0.9 (0–1.9)%. For the distorted subset, error was 6.3 (1.7–16.9)%. For type III episodes, error increased to 19.6 (7.7–40.3)%.

Table 1 shows the relation between the artifact type and the airway system, and the algorithm performance in the detection of overventilation alarms. Overall, type I artifact appeared in 48% of the distorted cases, type II in 21%, and type III in 31%

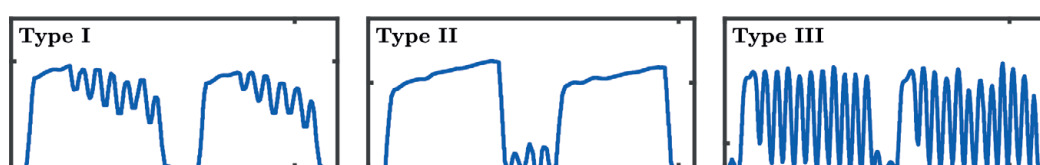


Figure 8. Intervals of chest compression oscillations observed in OHCA capnograms during ongoing CPR: type I, located in the plateau; type II, located in the baseline; type III, spanning from the plateau to the baseline.

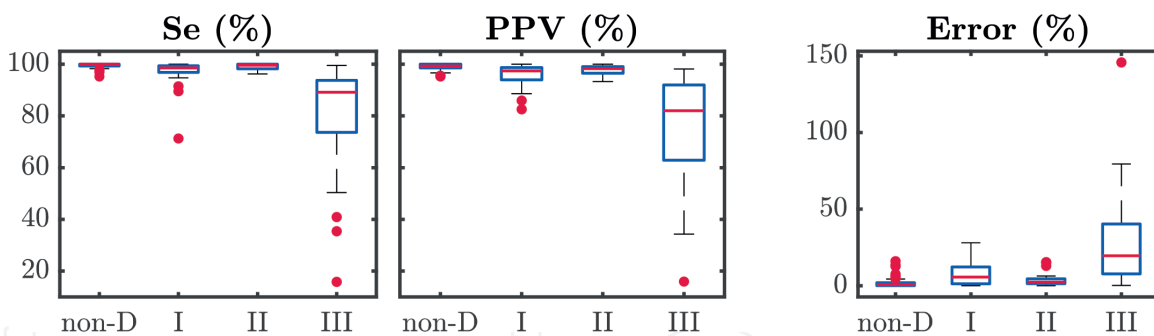


Figure 9. Automated ventilation detection performance and error in the estimation of ventilation rate. Results are provided for all categories: non-D, nondistorted; I, type I; II, type II; and III, type III.

| Group | Total | Ventilation type | | | | Gold standard | | Alarm detection | |
|-----------|-------|------------------|-----|-----|----|---------------|----------|-----------------|---------|
| | | BVM | ETT | SGA | NA | n_{vr} | n_{ov} | Se (%) | PPV (%) |
| Total | 232 | 7 | 149 | 73 | 3 | 31,760 | 17,901 | 99.1 | 92.6 |
| Non-D | 134 | 7 | 90 | 35 | 2 | 17,413 | 10,511 | 99.7 | 98.0 |
| Distorted | 98 | 0 | 59 | 38 | 1 | 14,347 | 7390 | 98.2 | 85.8 |
| Type I | 47 | 0 | 19 | 28 | 0 | 7167 | 3398 | 98.9 | 90.8 |
| Type II | 21 | 0 | 15 | 6 | 0 | 2826 | 1837 | 99.8 | 96.6 |
| Type III | 30 | 0 | 25 | 4 | 1 | 4354 | 2155 | 95.5 | 72.1 |

Non-D, nondistorted; BVM, bag valve mask; ETT, endotracheal tube; SGA, supraglottic airway; NA, not available; n_{vr} , number of ventilation rate per minute measurements annotated in the gold standard; n_{ov} , number of annotated overventilation alarms.

Table 1. Distribution of episodes according to artifact and airway type and algorithm performance in the detection of overventilation alarms.

of them. Artifact was not present where BVM ventilation was used, although the sample was small. However, all types of artifact appeared in both advanced airways, with a higher incidence for SGA cases. In ETT cases, incidence of type III artifact was more prevalent, whereas in SGA cases, type I was more prevalent.

There was a 56.4% (17,901/31,760) of 1-minute overventilation annotated intervals. Overventilation was accurately detected in the case of nondistorted episodes, but performance decreased in the distorted group (type III), particularly with respect to PPV.

4.4 Discussion

There is a lack of evidence about the incidence and origin of the chest compression artifact. One prior study has reported the impact of these induced oscillations on the capnogram during OHCA CPR. In this work, published as a conference abstract, Idris et al. [33] reported the appearance of oscillations in 154 episodes from a total of 210 OHCA records (73.3%). In our study, with a similar number of OHCA episodes (232 vs. 210), we found a lower incidence of distorted capnograms (42%). This could be explained by a different criterion for distorted episode classification.

Ventilation rate guidance is one of the emphasized advantages of capnography during OCHA episodes. However, the presence of fast oscillations in the capnogram during ongoing CPR may limit rescuers since distorted capnograms are difficult to interpret. Performed analyses demonstrated the negative impact of this artifact

in the detection of ventilations. Se and PPV were above 95%, and ventilation rate estimation errors were minimal for all the nondistorted episodes, but detection performance significantly decreased in the presence of oscillations. Thus, a reliable ventilation guidance would not be feasible for those OHCA patients.

Overventilation was common in our database: 56.4% of the annotated ventilation rates were above the recommended 10 breaths per minute. Sensitivity for alarm detection was high for all episodes (nondistorted and distorted). However, the algorithm showed a tendency to overestimate ventilation rate in the presence of chest compression oscillations, where PPV values were low. Induced oscillations spanning from the plateau to the baseline impeded a reliable detection of true ventilation CO₂ concentration changes. Hence, the presence of artifact in the waveform capnography caused many false ventilation detections.

5. Suppression of chest compression artifact during CPR

In Section 2 we quantitatively confirmed the nature of the oscillations, with a single frequency matching the chest compression rate, suggesting that the artifact is directly caused by ongoing chest compressions during CPR. In this context, we hypothesized that automatic ventilation detection would improve if the oscillations induced by chest compressions could be successfully removed from the capnogram. Our next step was designing chest compression artifact suppression techniques, exploring different alternatives.

5.1 Frequency domain filtering techniques

The following section describes the filtering techniques used for the suppression of the chest compression oscillations induced in the capnogram. We studied three different alternatives: a simple fixed-coefficient filter and two computationally intensive adaptive filtering techniques. To assess the goodness of the filter, we computed the performance using an automated capnogram-based ventilation detector after filtering OHCA capnograms. We also evaluated the improvement in ventilation rate measurement and in overventilation alarm detection. Then, we compared these results with those obtained before filtering, described previously in Section 4.4.

5.1.1 Fixed-coefficient filter

The spectral analysis performed on OHCA capnograms (see Section 3, **Figure 5**) suggests that a sensible strategy to suppress the oscillations induced by chest compressions in the capnogram would be to use a simple fixed-coefficient filter that suppresses the spectral content of the capnogram above 1 Hz (compression rate above 60 cpm). To that end, after analyzing the spectral characteristics of several waveform capnography and CD signals, we developed a digital infinite impulse response low-pass Butterworth filter (8th order, cutoff frequency of 1.5 Hz).

5.1.2 Adaptive filtering

Efficacy of the fixed-coefficient filter may be affected by the variability of chest compression and ventilation rates during CPR [17, 18, 30, 42]. In the literature, filters adjusted in time, according to the varying characteristics of the artifact, have been extensively used to suppress oscillations in the electrocardiogram induced by chest compressions [43–46]. In this study, we designed two adaptive filtering

configurations, an open-loop and a closed-loop adaptive filter [47]. Both techniques used the annotated chest compression instances, obtained from the CD signal as a reference to adjust the parameters of the adaptive filters. To do so, chest compression instances were annotated at the local minima as shown in **Figure 6** (top panel), corresponding to the maximum depth achieved for each chest compression. For more details of the adaptive filters, see Ref. [48].

Open-loop adaptive filter. This technique is based on the adaptive adjustment of a stop-band Butterworth filter whose central frequency is adaptively adjusted to the chest compression rate. Average chest compression rate was estimated in 2-s nonoverlapped windows, using the annotated chest compression instances. Thus, filter parameters were updated every 2 s.

Closed-loop adaptive filter. In our approach, the required reference signal was modeled as a pure cosine wave of time-varying amplitude and phase, estimating the instantaneous chest compression rate from the chest compression instances. In this configuration, the artifact is adaptively estimated and subtracted from the capnogram, resulting in an equivalent notch filter capable of adaptively tracking the chest compression oscillation frequency.

5.1.3 Results

The three proposed filter schemes performed similarly, reporting favorable global Se and PPV values well above 97 and 96%, respectively, for the distorted episodes, and maintaining the performance for nondistorted episodes. For this reason, and trying to keep this section as simple as possible, results for the closed-loop filter are reported. These results are representative of the three approaches. Readers are encouraged to see full results in Ref. [48].

Globally, Se/PPV improved from 96.4/95.0% before filtering to 98.2/98.3%. Performance improvement for type III episodes was remarkably higher, with Se/PPV improving from a low 77.6/73.5% to 95.5/95.5%. **Figure 10** (left panels) shows, for each artifact type, the distribution of Se and PPV per episode, before and after filtering. In the case of type III episodes, the high dispersion in performance was drastically reduced after artifact suppression. Box plots in **Figure 10** (right panel) show the distribution of error in the estimation of ventilation rate before and after filtering. In the same way, estimation error for type III episodes noticeably decreased after filtering.

Table 2 shows the performance improvement in the detection of overventilation. Globally, Se/PPV improved from 99.1/92.6% before filtering to 97.9/98.0%

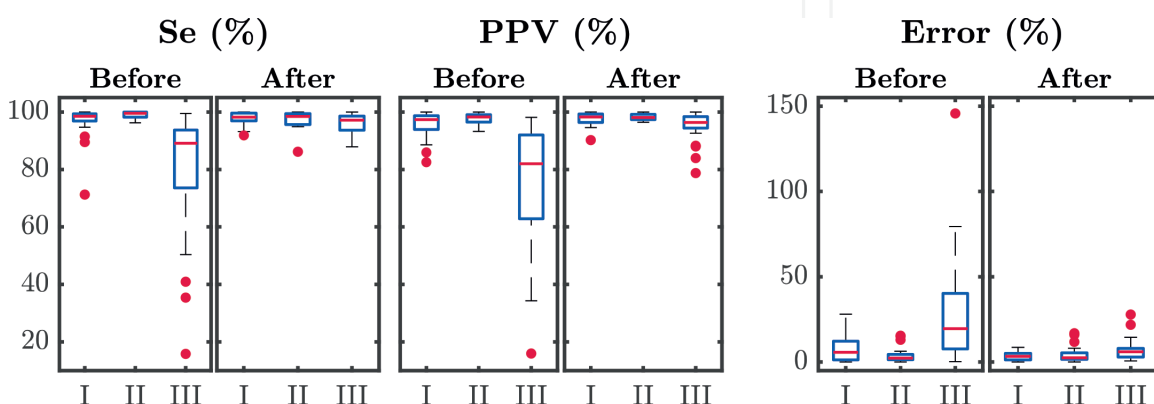


Figure 10. Se and PPV distribution per episode before and after filtering (left). Distribution of the unsigned error in the ventilation rate estimation (right). Results are provided for each artifact category: I, type I artifact; II, type II artifact; and III, type III artifact.

| Group | Gold standard | | Before | | After | |
|--------------|---------------|----------|--------|---------|--------|---------|
| | n_{vr} | n_{ov} | Se (%) | PPV (%) | Se (%) | PPV (%) |
| Total | 31,760 | 17,901 | 99.1 | 92.6 | 97.9 | 98.0 |
| Nondistorted | 17,413 | 10,511 | 99.7 | 98.0 | 98.9 | 98.9 |
| Distorted | 14,347 | 7390 | 98.2 | 85.8 | 96.3 | 96.6 |
| Type I | 7167 | 3398 | 98.9 | 90.8 | 98.0 | 97.0 |
| Type II | 2826 | 1837 | 99.8 | 96.6 | 95.2 | 98.3 |
| Type III | 4354 | 2155 | 95.5 | 72.1 | 94.8 | 94.2 |

n_{vr} , number of ventilation rate per minute measurements annotated in the gold standard; n_{ov} , number of annotated overventilation alarms.

Table 2.
Performance in the detection of overventilation alarms before and after filtering.

after filtering. Although the improvement for the distorted group was noticeable in all cases, improvement was remarkably higher for type III episodes, with Se/PPV of 95.5/72.1% before and 94.8/94.2% after filtering.

A graphical example of the closed-loop filtering approach is illustrated in **Figure 11**. The raw capnogram is depicted by the solid gray line and the resulting waveform capnography after filtering by the solid blue superimposed to the raw capnogram. Each vertical dashed red line indicates a detection of ventilation given by the automated ventilation detector.

5.1.4 Discussion

The presented filtering techniques were designed to preprocess the raw capnogram before applying the ventilation detection algorithm with the aim of improving automated ventilation detection. Although the closed-loop approach showed a great balance in Se and PPV improvement, none of the techniques showed a distinctive superiority in terms of performance. Since chest compression rates tend to vary during CPR, one could expect that adaptive filters would present better results than a simple fixed-coefficient filter, but this was not the case. This could be explained in part because chest compression rate is usually ten times greater than ventilation rate; thus spectral information is far away from one another. The selection of the filtering strategy could be analyzed in terms of simplicity and computational burden. Consequently, applying a simple fixed-coefficient filter to remove the chest compression artifact seems to be adequate.

As illustrated in **Figure 11**, resulting waveform capnography obtained after filtering approximates the mean peak-to-peak amplitude of the artifact. After

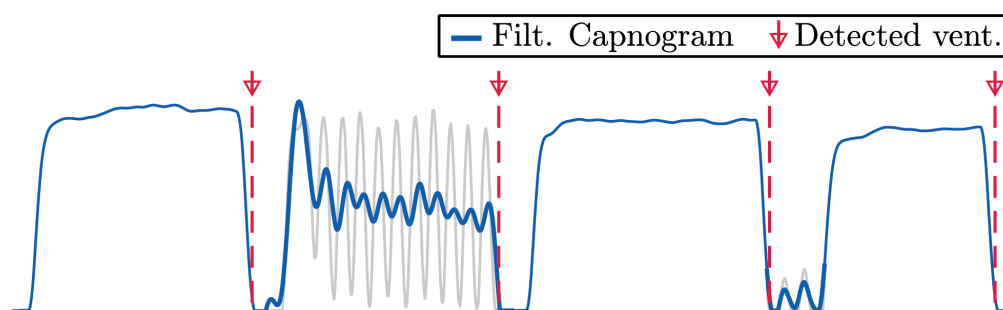


Figure 11.
Example of filtering performance. Original capnogram with clean and distorted respiration cycles is depicted by the solid gray line. Filtered capnogram (in blue) superimposed to the original capnogram. Detected ventilations are depicted with vertical dashed red lines.

filtering, output capnogram waveform hinders the ETCO_2 measurement and a reliable analysis of ETCO_2 trends. Thus, clinicians may still find the capnogram difficult to interpret. Removing the artifact to improve ventilation detection and at the same time preserving the capnogram tracing, which favors clinical interpretation, require the development of new suppressing techniques.

5.2 Time-domain artifact suppression technique

In the previous section, we proposed a solution to suppress chest compression artifact from the waveform capnography using different filtering approaches. Although the automated detection of ventilations was improved, filtered capnograms were far from being clinically reliable.

This section explores an alternative method to remove chest compression oscillations from the waveform capnography signal. This technique was designed to improve ventilation detection focusing on the real tracing preservation. Again, performance metrics previously described in the chapter were used for quantitatively assessing the goodness of the method. This study was conducted using the test subset described in Section 4.4.

5.2.1 Envelope detection algorithm

The principle of this artifact suppression technique relies on the hypothesis that the envelope of the waveform capnography signal could be a clinically reliable estimation of the CO_2 concentration tracing produced by ventilations. Due to artifact morphology and location variability reported in Section 4, the algorithm determines how to extract the envelope of the waveform capnography dividing its operation into low and high CO_2 concentration intervals.

A graphical explanation of the method's performance is given in **Figure 12**. To extract the upper envelope of the capnogram (dashed blue line), the algorithm detects the local maxima values (downward arrowheads) during the plateau phase and applies a smoothing filter. Then, in order to extract the lower envelope (dotted blue line), local minima values (upward arrowheads) are detected during the capnogram baseline. A detailed explanation of the algorithm is provided in Ref. [49].

5.2.2 Results

Globally, performance of the automated ventilation detection in terms of Se/PPV improved from 96.4/95.0% to 98.5/98.3% after artifact suppression.

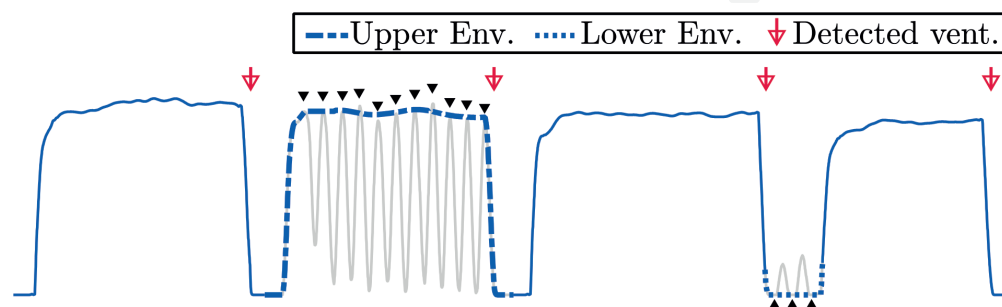


Figure 12.

Chest compression artifact suppression example. A distorted capnogram interval is depicted by the gray line. The blue line illustrates the waveform capnography envelope extraction process. Upper envelope (dashed blue line) is extracted through the detection of each local maxima (downward arrowheads), and lower envelope (dotted blue line) is extracted through the detection of each local minima (upward arrowheads). Detected ventilations are depicted with vertical red arrows.

Performance for nondistorted episodes stayed stable, whereas Se/PPV for distorted episodes increased noticeably, from 91.9/89.5% to 98.0/97.3%. As it happens with previous filtering methods, performance improved more in type III episodes, with Se/PPV increasing from 77.6/73.5% to 97.1/96.1%. **Figure 13** (left panels) depicts trough box plots, for each artifact type, the distribution of Se and PPV per episode given by the automated ventilation detector. In general, median values of both performance metrics increased after artifact suppression, and dispersion was reduced for all groups. These improvements were more noticeable for type III episodes. Performance regarding ventilation rate estimation is shown in **Figure 13** (right panel), in which box plots depict the distribution of the error before and after applying the suppression method. Errors were reduced in all groups, but again, improvements in case of type III episodes were noticeably higher.

Results after artifact suppression in the detection of excessive ventilation rates are reported in **Table 3**. In this case, Se stayed almost stable with a higher increase for PPV values. For the distorted subset, Se/PPV was 98.8/86.7% before and 98.4/96.3% after suppressing the artifact, implying a reduction in false overventilation alarms. Once again, most remarkable results were obtained for type III episodes, with a slight increase in Se, but with PPV increasing from 73.9 to 93.6% after artifact suppression.

Finally, performance of the suppression method is illustrated in **Figure 14**. The raw capnogram is depicted by a solid gray line and the resulting waveform capnography by a solid blue line superimposed to the raw capnogram.

5.2.3 Discussion

Filtering methods to remove the oscillations from the capnogram, described in Section 4, improved ventilation detection accuracy. However, filtered capnograms do not accurately represent the CO₂ concentration in intervals where the artifact appeared. In this section, a method that tries to preserve the waveform capnography has been proposed. Automated detection of ventilation instances, as well as estimation of ventilation rate and detection of overventilation, improved after artifact suppression. Results obtained with this method were similar or even better than the result reported for several filtering methods (Section 4).

The idea of “preserving the capnogram waveform” refers to the extraction of a clinically useful capnogram. We visually analyzed several capnogram segments in our database showing consecutive intervals with nondistorted and distorted ventilations (**Figure 14**). In most cases, the envelope of the distorted capnogram

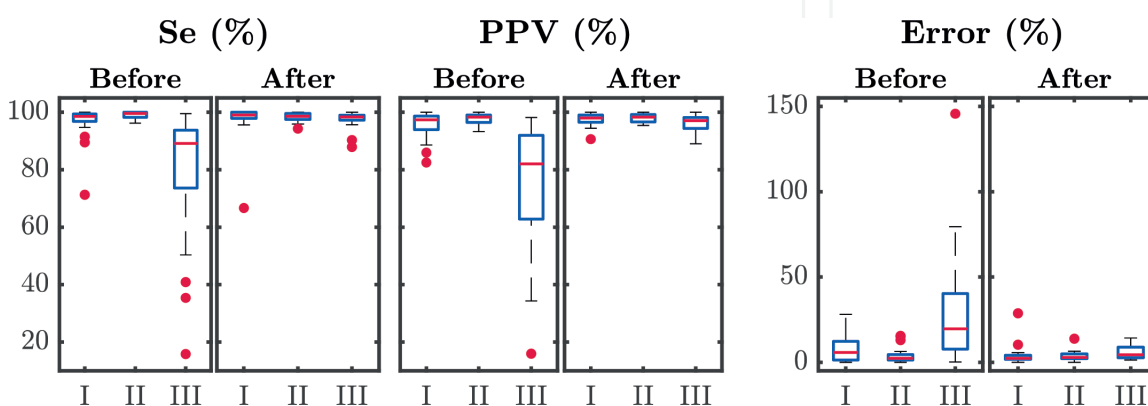


Figure 13. Se and PPV distribution per episode before and after artifact suppression method (left). Distribution of the unsigned error in the ventilation rate estimation (right). Results are provided for each artifact category: I, type I artifact; II, type II artifact; and III, type III artifact.

| Group | Total | Gold standard | | Before | | After | |
|--------------|-------|---------------|----------|--------|---------|--------|---------|
| | | n_{vr} | n_{ov} | Se (%) | PPV (%) | Se (%) | PPV (%) |
| Total | 202 | 25,833 | 15,237 | 99.3 | 93.1 | 98.9 | 97.8 |
| Nondistorted | 119 | 14,889 | 8873 | 99.7 | 98.2 | 99.3 | 98.9 |
| Distorted | 83 | 10,944 | 6364 | 98.8 | 86.7 | 98.4 | 96.3 |
| Type I | 42 | 5823 | 2961 | 99.1 | 90.7 | 98.7 | 97.2 |
| Type II | 16 | 2160 | 1570 | 99.8 | 97.8 | 97.5 | 97.7 |
| Type III | 25 | 2961 | 1833 | 97.2 | 73.9 | 98.7 | 93.6 |

n_{vr} , number of ventilation rate per minute measurements annotated in the gold standard; n_{ov} , number of annotated overventilation alarms.

Table 3.
 Overventilation alarm detection performance before and after applying the artifact suppression method.

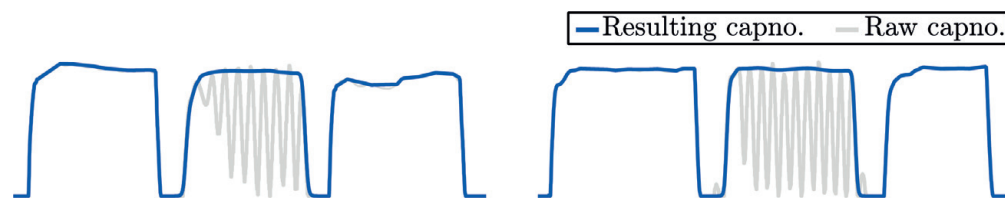


Figure 14.
 Examples of artifact suppression method performance. Original capnogram with clean and distorted respiration cycles is depicted by the solid gray line. Filtered capnogram (in blue) superimposed to the original capnogram.

resembled the CO₂ tracing observed in the preceding and following undistorted respiratory cycles. Therefore, this method could enhance capnographs not accounting for the chest compression artifact effect.

6. Conclusions

Current resuscitation guidelines emphasize the use of waveform capnography during CPR in order to enhance CPR quality and improve patient outcomes. However, the first study presented in this chapter showed that ventilation rate and overventilation prevention were compromised by the high incidence of chest compression artifact. The appearance of artifact during ongoing CPR is unpredictable, and thus suppression algorithms that continuously process the raw capnogram could be a great approach for waveform capnography enhancement. All artifact suppression approaches yielded good performance in terms of sensitivity and positive predictive value figures of merit. However, the time-domain alternative was the only one that enhanced the capnogram tracing, favoring its interpretation during CPR. The implementation of artifact suppression techniques in current capnographs could increase the use of capnography in OHCA episodes, which could in turn contribute to improving CPR quality.

Acknowledgements

This work received financial support from the Basque Government (Basque Country, Spain) through the project IT1087-16 and the predoctoral research grant PRE-2017-2-0201.

The authors thank the TVF&R emergency medical service providers for collecting the out-of-hospital cardiac arrest episodes used in this study.

Conflict of interest

The authors declare no conflicts of interest.

IntechOpen

IntechOpen

Author details

Mikel Leturiondo*, Sofía Ruiz de Gauna, José Julio Gutiérrez, Digna M. González-Otero, Jesus M. Ruiz, Luis A. Leturiondo and Purificación Saiz
University of the Basque Country (UPV/EHU), Bilbao, Spain

*Address all correspondence to: mikel.leturiondo@ehu.eus

IntechOpen

© 2019 The Author(s). Licensee IntechOpen. This chapter is distributed under the terms of the Creative Commons Attribution License (<http://creativecommons.org/licenses/by/3.0>), which permits unrestricted use, distribution, and reproduction in any medium, provided the original work is properly cited. 

References

- [1] Mehra R. Global public health problem of sudden cardiac death. *Journal of Electrocardiology*. 2007;**40**(6):S118-S122
- [2] Katritsis DG, Gersh BJ, Camm AJ. A clinical perspective on sudden cardiac death. *Arrhythmia & Electrophysiology Review*. 2016;**5**(3):177
- [3] Myerburg RJ, Kessler KM, Castellanos A. Sudden cardiac death. Structure, function, and time-dependence of risk. *Circulation*. 1992;**85**(1 Suppl):I2-I10
- [4] Kannel WB, Schatzkin A. Sudden death: Lessons from subsets in population studies. *Journal of the American College of Cardiology*. 1985;**5**(6 Supplement 1):141B-149B
- [5] Atwood C, Eisenberg MS, Herlitz J, Rea TD. Incidence of EMS-treated out-of-hospital cardiac arrest in Europe. *Resuscitation*. 2005;**67**(1):75-80
- [6] Nichol G, Baker D. The epidemiology of sudden death. In: Paradir NA, Halperin HR, Kern KB, Wenzel V, Chamberlain D, editors. *Cardiac Arrest: Science and Practice of Resuscitation Medicine*. Cambridge: Cambridge University Press; 2007. pp. 26-50
- [7] Soar J, Nolan JP, Böttiger BW, Perkins GD, Lott C, Carli P, et al. European Resuscitation Council guidelines for resuscitation 2015. Section 3. Adult advanced life support. *Resuscitation*. 2015;**95**:100-147
- [8] Link MS, Berkow LC, Kudenchuk PJ, Halperin HR, Hess EP, Moitra VK, et al. 2015 American Heart Association Guidelines Update for Cardiopulmonary Resuscitation and Emergency Cardiovascular Care. Part 7: Adult advanced cardiovascular life support. *Circulation*. 2015;**132** (18 suppl 2):S444-S464
- [9] Idris AH, Guffey D, Aufderheide TP, Brown S, Morrison LJ, Nichols P, et al. Relationship between chest compression rates and outcomes from cardiac arrest. *Circulation*. 2012;**125**:3004-3012
- [10] Edelson DP, Abella BS, Kramer-Johansen J, Wik L, Myklebust H, Barry AM, et al. Effects of compression depth and pre-shock pauses predict defibrillation failure during cardiac arrest. *Resuscitation*. 2006;**71**(2):137-145
- [11] Kramer-Johansen J, Myklebust H, Wik L, Fellows B, Svensson L, Sørebo H, et al. Quality of out-of-hospital cardiopulmonary resuscitation with real time automated feedback: A prospective interventional study. *Resuscitation*. 2006;**71**(3):283-292
- [12] Monsieurs KG, Nolan JP, Bossaert LL, Greif R, Maconochie IK, Nikolaou NI, et al. European resuscitation council guidelines for resuscitation 2015: Section 1. Executive summary. *Resuscitation*. 2015;**95**:1-80
- [13] Berg RA, Hemphill R, Abella BS, Aufderheide TP, Cave DM, Hazinski MF, et al. Part 5: Adult basic life support: 2010 American Heart Association Guidelines for Cardiopulmonary Resuscitation and Emergency Cardiovascular Care. *Circulation*. 2010;**122**(18 Suppl 3):S685-S705
- [14] Pitts S, Kellermann AL. Hyperventilation during cardiac arrest. *Lancet*. 2004;**364**(9431):313-315
- [15] Benoit JL, Prince DK, Wang HE. Mechanisms linking advanced airway management and cardiac arrest outcomes. *Resuscitation*. 2015;**93**:124-127
- [16] Aufderheide TP, Sigurdsson G, Pirralo RG, Yannopoulos D, McKnite S, von Briesen C, et al.

Hyperventilation-induced hypotension during cardiopulmonary resuscitation. *Circulation*. 2004;**109**(16):1960-1965

[17] O'Neill JF, Deakin CD. Do we hyperventilate cardiac arrest patients? *Resuscitation*. 2007;**73**(1):82-85

[18] Maertens VL, De Smedt LE, Lemoyne S, Huybrechts SA, Wouters K, Kalmar AF, et al. Patients with cardiac arrest are ventilated two times faster than guidelines recommend: an observational prehospital study using tracheal pressure measurement. *Resuscitation*. 2013;**84**(7):921-926

[19] Yannopoulos D, McKnite S, Aufderheide TP, Sigurdsson G, Pirralo RG, Benditt D, et al. Effects of incomplete chest wall decompression during cardiopulmonary resuscitation on coronary and cerebral perfusion pressures in a porcine model of cardiac arrest. *Resuscitation*. 2005;**64**(3):363-372

[20] Aufderheide TP, Lurie KG. Death by hyperventilation: A common and life-threatening problem during cardiopulmonary resuscitation. *Critical Care Medicine*. 2004;**32**(9):S345-S351

[21] Silvestri S, Ralls GA, Krauss B, Thundiyil J, Rothrock SG, Senn A, et al. The effectiveness of out-of-hospital use of continuous end-tidal carbon dioxide monitoring on the rate of unrecognized misplaced intubation within a regional emergency medical services system. *Annals of Emergency Medicine*. 2005;**45**(5):497-503

[22] Qvigstad E, Kramer-Johansen J, Tømte Ø, Skålhegg T, Sørensen Ø, Sunde K, et al. Clinical pilot study of different hand positions during manual chest compressions monitored with capnography. *Resuscitation*. 2013;**84**(9):1203-1207

[23] Pokorná M, Nečas E, Kratochvíl J, Skřipický R, Andrlík M, Franěk O. A

sudden increase in partial pressure end-tidal carbon dioxide (PETCO₂) at the moment of return of spontaneous circulation. *The Journal of Emergency Medicine*. 2010;**38**(5):614-621

[24] Kodali BS, Urman RD, et al. Capnography during cardiopulmonary resuscitation: Current evidence and future directions. *Journal of Emergencies, Trauma, and Shock*. 2014;**7**(4):332

[25] Touma O, Davies M. The prognostic value of end tidal carbon dioxide during cardiac arrest: A systematic review. *Resuscitation*. 2013;**84**(11):1470-1479

[26] Jaffe MB. Infrared measurement of carbon dioxide in the human breath: "Breathe-through" devices from Tyndall to the present day. *Anesthesia and Analgesia*. 2008;**107**(3):890-904

[27] Bhavani-Shankar K, Philip JH. Defining segments and phases of a time capnogram. *Anesthesia and Analgesia*. 2000;**91**(4):973-977

[28] Gravenstein JS, Jaffe MB, Gravenstein N, Paulus DA. Capnography. In: Gravenstein JS, editor. *Clinical Perspectives*. Cambridge: Cambridge University Press; 2011. pp. 6-9

[29] Pantazopoulos C, Xanthos T, Pantazopoulos I, Papalois A, Kouskouni E, Iacovidou N. A review of carbon dioxide monitoring during adult cardiopulmonary resuscitation. *Heart, Lung & Circulation*. 2015;**24**(11):1053-1061

[30] Meaney PA, Bobrow BJ, Mancini ME, et al. Cardiopulmonary resuscitation quality: Improving cardiac resuscitation outcomes both inside and outside the hospital: A consensus statement from the American Heart Association. *Circulation*. 2013;**128**(4):417-435

- [31] Takla G, Petre JH, Doyle DJ, Horibe M, Gopakumaran B. The problem of artifacts in patient monitor data during surgery: A clinical and methodological review. *Anesthesia and Analgesia*. 2006;**103**(5):1196-1204
- [32] Herry CL, Townsend D, Green GC, Bravi A, Seely AJE. Segmentation and classification of capnograms: Application in respiratory variability analysis. *Physiological Measurement*. 2014;**35**(12):2343
- [33] Idris AH, Daya M, Owens P, et al. High incidence of chest compression oscillations associated with capnography during out-of-hospital cardiopulmonary resuscitation. *Circulation*. 2010;**122**:A83
- [34] Deakin CD, O'Neill JF, Tabor T. Does compression-only cardiopulmonary resuscitation generate adequate passive ventilation during cardiac arrest? *Resuscitation*. 2007;**75**(1):53-59
- [35] Vanwulpen M, Wolfskeil M, Duchatelet C, Monsieurs K, Idrissi SH. Quantifying inspiratory volumes generated by manual chest compressions during resuscitation in the prehospital setting. *Resuscitation*. 2017;**118**:e18
- [36] Idris AH, Banner MJ, Wenzel V, Fuerst RS, Becker LB, Melker RJ. Ventilation caused by external chest compression is unable to sustain effective gas exchange during CPR: A comparison with mechanical ventilation. *Resuscitation*. 1994;**28**(2):143-150
- [37] Leturiondo M, de Gauna SR, Ruiz JM, Gutiérrez JJ, Leturiondo LA, González-Otero DM, et al. Influence of chest compression artefact on capnogram-based ventilation detection during out-of-hospital cardiopulmonary resuscitation. *Resuscitation*. 2018;**124**:63-68
- [38] Raimondi M, Savastano S, Pamploni G, Molinari S, Degani A, Belliato M. End-tidal carbon dioxide monitoring and load band device for mechanical cardio-pulmonary resuscitation: Never trust the numbers, believe at the curves. *Resuscitation*. 2016;**103**:e9-e10
- [39] Pellis T, Bisera J, Tang W, Weil MH. Expanding automatic external defibrillators to include automated detection of cardiac, respiratory, and cardiorespiratory arrest. *Critical Care Medicine*. 2002;**30**(4):S176-S178
- [40] Losert H, Risdal M, Sterz F, Nysaether J, Koehler K, Eftestøl T, et al. Thoracic impedance changes measured via defibrillator pads can monitor ventilation in critically ill patients and during cardiopulmonary resuscitation. *Critical Care Medicine*. 2006;**34**(9):2399-2405
- [41] Edelson DP, Eilevstjønn J, Weidman EK, Retzer E, Hoek TLV, Abella BS. Capnography and chest-wall impedance algorithms for ventilation detection during cardiopulmonary resuscitation. *Resuscitation*. 2010;**81**(3):317-322
- [42] Abella BS, Sandbo N, Vassilatos P, Alvarado JP, O'hearn N, Wigder HN, et al. Chest compression rates during cardiopulmonary resuscitation are suboptimal: A prospective study during in-hospital cardiac arrest. *Circulation*. 2005;**111**(4):428-434
- [43] Aase SO, Eftestøl T, Husøy JH, Sunde K, Steen PA. CPR artifact removal from human ECG using optimal multichannel filtering. *IEEE Transactions on Biomedical Engineering*. 2000;**47**(11):1440-1449
- [44] Eilevstjønn J, Eftestøl T, Aase SO, Myklebust H, Husøy JH, Steen PA. Feasibility of shock advice analysis during CPR through removal of CPR artefacts from the human ECG. *Resuscitation*. 2004;**61**(2):131-141

[45] Gong Y, Chen B, Li Y. A review of the performance of artifact filtering algorithms for cardiopulmonary resuscitation. *Journal of Healthcare Engineering*. 2013;**4**(2):185-202

[46] Ruiz de Gauna S, Irusta U, Ruiz J, Ayala U, Aramendi E, Eftestøl T. Rhythm analysis during cardiopulmonary resuscitation: Past, present, and future. *BioMed Research International*. 2014;**2014**:1-13

[47] Widrow B, Stearns SD. *Adaptive Signal Processing*. Vol. 1. Englewood Cliffs, NJ: Prentice-Hall, Inc; 1985. p. 491

[48] Gutiérrez JJ, Leturiondo M, Ruiz de Gauna S, Ruiz JM, Leturiondo LA, et al. Enhancing ventilation detection during cardiopulmonary resuscitation by filtering chest compression artifact from the capnography waveform. *PLoS One*. 2018;**13**(8):e0201565

[49] Ruiz de Gauna S, Leturiondo M, Gutiérrez JJ, Ruiz JM, González-Otero DM, Russell JK, et al. Enhancement of capnogram waveform in the presence of chest compression artefact during cardiopulmonary resuscitation. *Resuscitation*. 2018;**133**:53-58